

# Ionic conductivity and thermal stability of magnetron-sputtered nanocrystalline yttria-stabilized zirconia

**Sillassen, M.; Eklund, P.; Sridharan, M.; Pryds, Nini; Bonanos, Nikolaos; Bøttiger, J.**

*Published in:*
Journal of Applied Physics

*Link to article, DOI:*
10.1063/1.3130404

*Publication date:*
2009

*Document Version*
Publisher's PDF, also known as Version of record

# Ionic conductivity and thermal stability of magnetron-sputtered nanocrystalline yttria-stabilized zirconia

M. Sillassen,[1,a)] P. Eklund,[1,2] M. Sridharan,[1,b)] N. Pryds,[3] N. Bonanos,[3] and J. Bøttiger[1]
[1]*Department of Physics and Astronomy and Interdisciplinary Nanoscience Center (iNANO), University of Aarhus, DK-8000 Aarhus C, Denmark*
[2]*Department of Physics, Chemistry, and Biology, Thin Film Physics Division, IFM, Linköping University, S-581 83 Linköping, Sweden*
[3]*Fuel Cells and Solid State Chemistry Division, Risø National Laboratory for Sustainable Energy, Technical University of Denmark (DTU), DK-4000 Roskilde, Denmark*

(Received 9 December 2008; accepted 11 April 2009; published online 22 May 2009)

Thermally stable, stoichiometric, cubic yttria-stabilized zirconia (YSZ) thin-film electrolytes have been synthesized by reactive pulsed dc magnetron sputtering from a Zr–Y (80/20 at. %) alloy target. Films deposited at floating potential had a ⟨111⟩ texture. Single-line profile analysis of the 111 x-ray diffraction peak yielded a grain size of ~20 nm and a microstrain of ~2% regardless of deposition temperature. Films deposited at 400 °C and selected bias voltages in the range from −70 to −200 V showed a reduced grain size for higher bias voltages, yielding a grain size of ~6 nm and a microstrain of ~2.5% at bias voltages of −175 and −200 V with additional incorporation of argon. The films were thermally stable; very limited grain coarsening was observed up to an annealing temperature of 800 °C. Temperature-dependent impedance spectroscopy analysis of the YSZ films with Ag electrodes showed that the in-plane ionic conductivity was within one order of magnitude higher in films deposited with substrate bias corresponding to a decrease in grain size compared to films deposited at floating potential. This suggests that there is a significant contribution to the ionic conductivity from grain boundaries. The activation energy for oxygen ion migration was determined to be between 1.14 and 1.30 eV. © *2009 American Institute of Physics*. [DOI: 10.1063/1.3130404]

## I. INTRODUCTION

In conventional solid oxide fuel cells (SOFCs), the electrolyte material of choice is yttria-stabilized zirconia (YSZ).[1,2] YSZ is relatively cheap to process, an acceptable ionic conductor, chemically inert, nontoxic, and has sufficiently low electronic conductivity to avoid any short circuiting of the cell. The ionic conductivity in the stabilized zirconia system is due to the mobility of oxygen vacancies created by doping with an element of lower valence. In SOFCs, the typical thickness of the electrolyte layer is of the order of 10–100 $\mu$m. A way of lowering the operation temperature of SOFCs could be to implement thin-film electrolytes ($<1$ $\mu$m) in order to minimize the Ohmic losses;[3] alternatively the ionic conductivity can be increased by increasing the mobility of the ionic species. A number of studies of the mechanisms for ionic conduction in nanomaterials[4–7] have shown that the migration of ions is mainly affected by grain boundaries and interfaces, which can exhibit orders of magnitude greater diffusivity than that of the lattice.[8,9] The potential of these nanomaterials indicates the importance of nanoionics.[10,11]

Both chemical and physical vapor deposition (PVD) techniques have been used to synthesize YSZ thin films. Among the PVD methods, rf sputtering,[12] pulsed laser deposition,[13–15] and reactive sputtering[16,17] have been the most widely used. In the present paper, we correlate the structure and in-plane ionic conductivities of nanocrystalline YSZ thin films synthesized by reactive pulsed dc magnetron sputtering. The activation energy for oxygen ion migration was between 1.14–1.30 eV, similar to reported values for bulk migration in YSZ. The absolute values of the ionic conductivity as a function of the grain size suggest that migration along grain boundaries also contributes to the ionic conduction.

## II. EXPERIMENTAL DETAILS

YSZ films were deposited by reactive pulsed dc magnetron sputtering. Si(001) substrates ($15\times15$ mm$^2$) with native oxide layers were used. In addition, nonconducting quartz $SiO_2$(001) substrates ($20\times6$ mm$^2$) were used for the films intended for in-plane ionic conductivity measurements. All substrates were ultrasonically cleaned in acetone and ethanol and blown dry in nitrogen. The growth chamber was equipped with two unbalanced magnetron sources (AJA International, Inc.) each with a 50.8 mm (∅) Zr–Y alloy target (80–20 at. %) placed at a distance of 15 cm above the substrate and tilted 25° away from the substrate normal. Only one magnetron at a time was used during the experiments. The magnetron source was powered by a bipolar pulsed dc supply (Advanced Energy MDX 1 kW+Sparc-le V unit) with −220 V for 40 $\mu$s and +33 V for 10 $\mu$s, corresponding to a total period of 50 $\mu$s. As equal sputtering rates are

[a)]Author to whom correspondence should be addressed. Electronic mail: mbs@phys.au.dk.
[b)]Present address: Center for Nanotechnology and Advanced Biomaterials (CeNTAB), SASTRA University, Thanjavur 613 402, Tamil Nadu, India.

 

expected for Y and Zr during steady-state sputtering, this should give a film composition $(ZrO_2)_{0.89}(Y_2O_3)_{0.11}$ the composition of fully stabilized cubic zirconia at room temperature.

The chamber was equipped with a turbomolecular pump (550 l/s) by means of which a base pressure $\leq 10^{-5}$ Pa was obtained. A deposition rate of ~8 nm/min was obtained at a working pressure of 0.5 Pa with a gas mixture of Ar (99.9996%) and $O_2$ (99.9999%) with an Ar:$O_2$ flow ratio of 9:0.8 SCCM (SCCM denotes cubic centimeter per minute at STP). Due to a relatively low power density (~1.4 W/cm$^2$) to the target, hysteresis was observed when varying the oxygen content during the sputtering process. In order to have a stable process with a reasonably high deposition rate, films were synthesized in the metallic mode. The deposition times were 30 and 150 min corresponding to film thicknesses of ~230 nm and ~1.1 $\mu$m, respectively.

Substrates were mounted on a holder containing a resistive heater that allows the substrate temperature to be varied from room temperature to ~400 °C. The temperature was measured with a thermocouple embedded in the holder. In order to vary the incident flux and energy of the charged species bombarding the growing film, an effective dc bias was applied to the substrate by use of an rf power supply. A manual shutter protected the substrate before deposition.

The film thickness and chemical composition were determined by Rutherford backscattering spectroscopy (RBS) using 2 MeV $^4He^+$ ions and a scattering angle of 161°. The experimental data were simulated with the RUMP program.[18] Within the measurement accuracy, RBS showed that the film thickness had little dependence on substrate temperature (above 200 °C) and substrate bias. Furthermore, all films were found to be stoichiometric in oxygen. X-ray diffraction (XRD) measurements in $\theta$-$2\theta$ and grazing incidence x-ray diffraction (GIXRD) geometry (5° incidence) were performed with a Bruker D8 Discover diffractometer using Cu $K\alpha$ radiation. Single-line profile analysis was performed with the software package TOPAS 2.1 (Ref. 19) using a pseudo-Voigt peak profile;[20] the size of the coherently diffracting domains, which has been used as a measure for the average grain size, and the microstrain were determined from the integral breadths of the Lorentzian and Gaussian constituents of the pseudo-Voigt function, respectively. Scanning electron microscopy (SEM) was performed in an FEI NOVA 600 SEM with accelerating voltage of 5 kV and working distance of 4 mm. Transmission electron microscopy (TEM) was performed in a Philips CM20 TEM working at 200 kV.

Annealing was carried out in a quartz tube oven with a flow of pure nitrogen (1 l/min). The samples were placed on a quartz boat, which was placed at the center of the preheated oven and annealed for 1 h. The temperature was measured with a thermocouple placed near the samples inside the oven (error ± 10 °C). After annealing, the samples were cooled down for 1 h before they were taken out of the oven so the samples would not be exposed to thermal shock. This procedure was repeated for each annealing temperature in the range of 400–800 °C in steps of 100 °C.

Impedance spectroscopy measurements were carried out in a dry-air atmosphere oven using Ag electrodes painted onto the film surface. The YSZ films were ~1 $\mu$m thick on a quartz substrate and the separation between the Ag electrodes was 2 mm. Measurements were performed at temperatures from 650 down to 400 °C in steps of 50 °C (10 °C/min) and a dwell time of 40 min in order to avoid any microstructural changes between measurements and to ensure steady-state conditions at each measuring point. However, the sample deposited at 400 °C and −200 V bias was characterized while heating up to 650 °C since the film peeled off the substrate at the peak temperature. All the other samples showed good adhesion to the substrate. Annealing effects had a negligible influence on the impedance data obtained during a full thermal cycle (data not shown). A Hioki 3250-50 frequency analyzer in the range of 42 Hz–1 MHz was used and the impedance data were analyzed with the software ZSIMPWIN 3.21.[21]

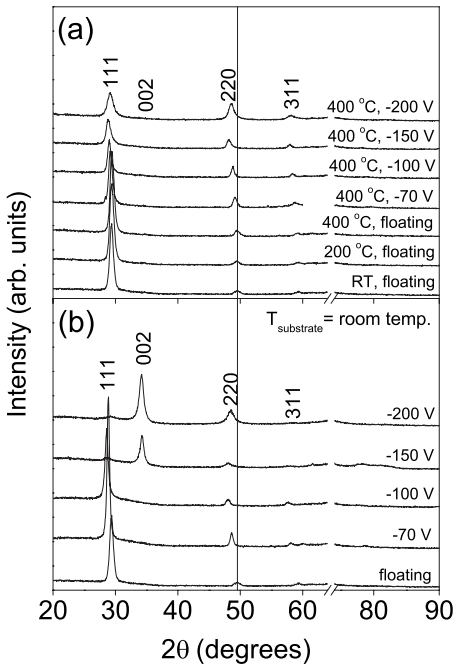


FIG. 1. (a) $\theta$-$2\theta$ x-ray diffractograms of YSZ samples deposited at different substrate temperatures and bias voltages. (b) $\theta$-$2\theta$ x-ray diffractograms of YSZ samples deposited at room temperature and various bias voltages. The indexed peaks correspond to the fcc-fluorite structure, but only the clearest peaks are indicated. The Si 004 substrate peak has been omitted.

## III. RESULTS AND DISCUSSION

### A. Structural analysis

Figures 1(a) and 1(b) show $\theta$-$2\theta$ x-ray diffractograms for films deposited at various substrate temperatures and bias voltages. All peaks can be attributed to cubic YSZ.[22] No tetragonal or monoclinic zirconia phase is seen. Furthermore, no amorphous material was observed in TEM (not shown). In Fig. 1(a), the 111 peak is dominant for films deposited at floating potential and room temperature, 200 and 400 °C, showing that these films have a ⟨111⟩ texture. At these temperatures and floating potential, the ⟨111⟩ film texture is likely to develop due to the low surface energies of ⟨111⟩ oriented grains, as known for fcc metals.[23,24] For samples deposited at 400 °C with applied biases of −70, −100,

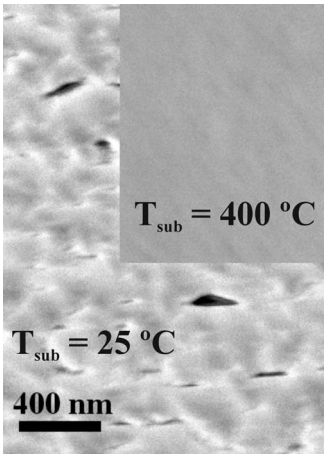


FIG. 2. SEM surface images of samples deposited at room temperature (main) and 400 °C (inset) at floating potential.

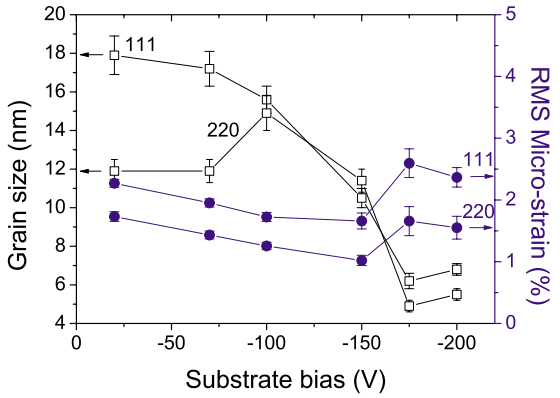


FIG. 3. (Color online) Grain size and microstrain vs substrate bias for 111 and 220 diffraction peaks obtained in the GIXRD geometry. The error bars represent the estimated standard deviations when fitting the x-ray data to a pseudo-Voigt function.

−150, and −200 V [Fig. 1(a)], a change in texture from (111) to (220) at higher bias is observed. The peak positions are systematically shifted toward lower $2\theta$ angles (i.e., larger out-of-plane lattice constants) for samples deposited at higher bias relative to the sample deposited at floating potential with higher bias yielding a larger peak shift, except for the sample deposited at −200 V where the peak shift (0.92° for 111 peak) is somewhat smaller than for the sample deposited at −150 V (1.32° for 111 peak).

Figure 1(b) shows $\theta$-$2\theta$ x-ray diffractograms for samples deposited at room temperature with and without applied bias. A strong ⟨111⟩ texture is observed for the sample deposited at floating potential [Fig. 1(b), bottom]. By applying a bias of −70 or −100 V during deposition, a ⟨111⟩ texture also developed in the films, and the peak positions are again seen to shift toward lower $2\theta$ angles. However, the samples deposited at −150 and −200 V biases developed a strong ⟨200⟩ texture [Fig. 1(b), top]. This texture change has also been reported by Yashar *et al.*[25] for YSZ films deposited onto steel substrates by pulsed dc reactive sputtering.

We attribute these texture changes to the increased ion bombardment during film deposition. Dobrev[26] showed that open lattice structures evolve under ion bombardment because of a lower sputtering yield for the more open directions, while Dong and Srolovitz[27] showed that a recrystallization mechanism due to ion-bombardment-induced lattice defects is more likely to explain the texture changes. These ion-bombardment effects explain why a ⟨200⟩ texture developed at high biases for samples deposited at room temperature since ⟨200⟩ provides an easy channeling direction in YSZ, resulting in less sputtering and a lower defect concentration. For the samples deposited at 400 °C, the mixed texture of ⟨111⟩ and ⟨220⟩ at high bias during growth is expected due to the balance between surface energy minimization and ion-induced texturing. The XRD peak positions for samples deposited at high bias may change due to an increased defect density, i.e., stress, originating from the ion bombardment.

The SEM micrographs in Fig. 2 show the surface morphologies for two samples deposited on quartz at floating potential at room temperature (main) and 400 °C (inset). For the film deposited at room temperature (25 °C), voids were observed between the columnar grains, while the sample deposited at 400 °C showed no visible voids. From cross section SEM (XSEM), columnar growth was observed along the substrate normal for both types of substrates (not shown).

For the 111 diffraction peaks from the $\theta$-$2\theta$ scans of the samples deposited at floating potential [Fig. 1(a)], the grain size and microstrain were ~20 nm and ~2%, respectively, regardless of deposition temperature. Figure 3 shows the grain sizes and microstrains determined from the 111 and 220 diffraction peaks (in GIXRD) for films deposited at 400 °C and floating potential (~−20 V) and bias voltages of −70, −100, −150, −175, and −200 V. At floating potential and at a bias of −70 V, the grain sizes for 111 and 220 diffraction peaks were ~18 and ~12 nm, respectively. However, at −100 V bias the 220 and 111 grains were both ~15 nm. This development is attributed to the texture change from the (111) surface to the (220) surface [cf. Fig. 1(a)], and the smaller grain size at high bias than at low bias is presumably due to the formation (by ion bombardment) of more nucleation centers. A grain size of ~6 nm for both diffraction peaks is found in films deposited at −175 and −200 V. Compared to the sample deposited at floating potential (−20 V), the microstrain decreased from ~2.3% down to ~1.7% for the sample deposited at −150 V evaluated for the 111 diffraction peak and from ~1.7% down to ~1.0% for the 220 diffraction peak. For samples deposited at a bias above −150 V, the bombarding $Ar^+$ ions induced radiation damage as indicated by the increase in microstrain (Fig. 3). No significant difference was observed in grain size and microstrain when comparing $\theta$-$2\theta$ and GIXRD data.

Figure 4 shows a logarithmic-scale plot of the RBS spectra for two samples deposited at floating potential and a bias of −200 V. The substrate temperature was 400 °C. A large Ar signal is seen for the sample deposited at −200 V. Generally, Ar impurities from the process gas were incorporated in the films when a substrate bias of −100 V or higher was applied during deposition. The sample at −100 V had an Ar content of ~0.5 at. %, just within the RBS detection limit. The samples deposited at −150, −175, and −200 V had Ar contents of 1.0, 1.7, and 1.5 at. %, respectively. The RBS

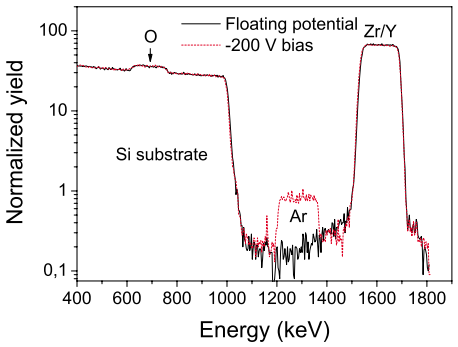


FIG. 4. (Color online) Log-scale plot of the RBS spectra from two YSZ films on Si deposited at 400 °C for 30 min at a floating substrate bias potential and a substrate bias of −200 V, respectively. An Ar impurity content of 1.5 at. % is observed in the −200 V film.

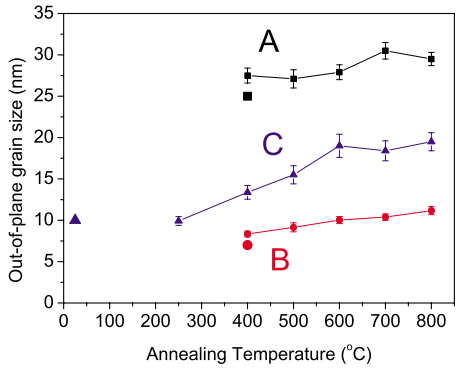


FIG. 6. (Color online) Grain growth from successive annealing. Big symbols denote the out-of-plane grain size as deposited. The sample deposited at room temperature had initially been annealed at 250 °C.

spectra in Fig. 4 show that the film thicknesses and the oxygen-to-metal ratio for the two samples are the same when comparing the respective widths and areas of the elemental signals. This observation indicates that resputtering is not a significant effect during growth. We attribute this to the high binding energies in zirconia compared to nonoxides.[28]

Figures 5(a) and 5(b) show the TEM images of the samples deposited at −150 and −200 V, respectively. For the sample at −200 V [Fig. 5(b)], bright spots along the grain boundaries and within the grains are observed. These spots are not as pronounced in the film at −150 V [Fig. 5(a)]. Supported by the RBS compositional results, the bright spots could be very small Ar bubbles dispersed throughout the film.

The structural analysis for YSZ films deposited on quartz (data not shown) revealed no significant differences from those deposited on Si.

### B. Thermal stability

The thermal stability was studied for three samples labeled A, B, and C. Sample A was deposited at 400 °C and floating potential and exhibited a preferred ⟨111⟩ orientation [Fig. 1(a)]; sample B was deposited at 400 °C and a bias of −200 V and exhibited a mixture of ⟨111⟩ and ⟨220⟩ orientations [Fig. 1(a)]; and sample C was deposited at room temperature and a bias of −200 V and exhibited a preferred ⟨200⟩ orientation [Fig. 1(b)]. Sample C was initially annealed at 250 °C for 1 h, while samples A and B were initially annealed at 400 °C for 1 h. All samples were annealed for 1 h at each annealing temperature in the range of 400–800 °C in steps of 100 °C.

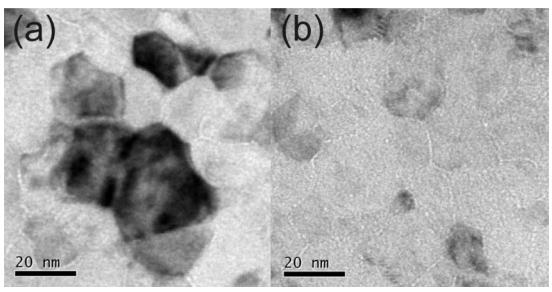


FIG. 5. Underfocused (bright-field) TEM images of the samples deposited at biases of (a) −150 and (b) −200 V. The picture in (b) shows a large quantity of tiny white dots, which are interpreted as small Ar bubbles.

The XRD scans obtained in both geometries (not shown) exhibited peaks from cubic YSZ for each annealing temperature. By annealing, the 111 peak positions shifted toward larger $2\theta$ values (0.45°) for samples deposited at −200 V bias (B and C). For sample A (deposited at floating potential), the 111 peaks only shifted to 0.17°. These observations are probably due to the fact that a large amount of lattice defects is inherent in samples B and C, as deposited, caused by the high energy ion bombardment. The defects are expected to anneal out at high temperatures, thereby relaxing the stress in the films. However, no evolution in microstrain was observed (data not shown), which may indicate that the defect structure changes from more pointlike defects to more extended defects (Ar bubbles, dislocation loops, etc.).

Figure 6 shows the grain growth from successive annealing of the films. The grain sizes were derived from single-line profile analysis of the strongest peaks obtained in the $\theta$-$2\theta$ geometry. For samples deposited at 400 °C (A and B), only limited grain growth was observed after annealing. However, in sample C the grain size increased by almost a factor of 2 as a result of annealing. These results indicate that the thermal stabilities in these samples are mainly dependent on the initial deposition temperature and not the applied bias voltage.

These annealing results are important because they show that negligible grain growth occurs below 800 °C for samples deposited at 400 °C. Therefore grain growth is not an issue for the ionic-conductivity measurements or for possible applications as thin-film electrolytes in SOFCs.

### C. In-plane ionic conductivity

Figure 7 shows the representative impedance spectra measured at 550 and 500 °C for an YSZ thin film deposited at −70 V and 400 °C. At all measured temperatures (650, 600, 550, 500, 450, and 400 °C), a single arc attributable to the sample was observed in the high-frequency end of the spectrum. The beginning of a second arc at low frequencies was due to the silver electrodes. In order to calculate the in-plane ionic conductivity, this type of response is interpreted and fitted according to the standard *RC*-circuit[29]

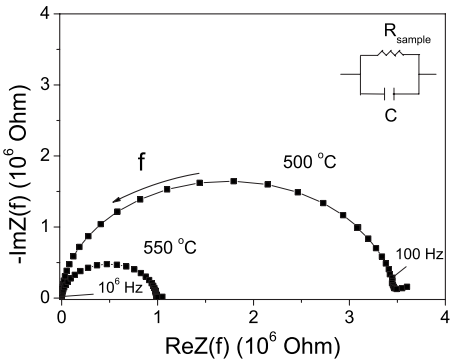


FIG. 7. Typical impedance spectra measured at 500 and 550 °C for a film with thickness $d=1$ $\mu$m deposited on quartz at 400 °C with a bias of −70 V. The frequency range used was 1 MHz–42 Hz.

shown in Fig. 7. The capacitance $C$ in this circuit is of the order of 10 pF, corresponding to the capacitance between the Ag electrodes and stray capacitance of the leads.

In these spectra a single depressed arc is observed, i.e., the semicircle is shifted below the real axis. This response is probably due to the superposition of several mechanisms for ionic conduction, i.e., bulk migration, grain boundary migration, etc. The expression relating to ionic conductivity $\sigma$ and absolute temperature $T$ is derived from the Nernst–Einstein relationship and is given by

$$\sigma T = A \exp(-E_a/k_B T), \tag{1}$$

where $A$ is the pre-exponential coefficient, $E_a$ is the activation energy for oxygen ion migration, and $k_B$ is the Boltzmann constant, respectively. Figure 8 shows the plots of $\log(\sigma T)$ versus $1000/T$ for samples deposited at floating potential and substrate temperatures of 200 and 400 °C, respectively, and samples deposited at 400 °C and bias voltages of −70, −100, and −200 V, respectively. All data sets follow an Arrhenius-type behavior. The in-plane ionic conductivities do not differ much for samples deposited at floating potential and substrate temperatures of 200 (solid squares) and 400 °C (open squares), respectively. However,

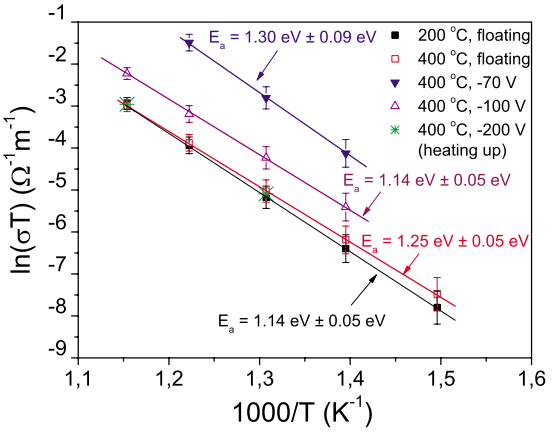


FIG. 8. (Color online) Arrhenius plots showing the in-plane ionic conductivity vs inverse temperature for films deposited at different substrate temperatures and bias voltage potentials. The sample deposited at 400 °C and −200 V bias was characterized while heating up to 650 °C. The error bars have been calculated from the measuring geometry and the standard deviation of the resistance.

by applying a substrate bias during deposition an increase in the in-plane ionic conductivity by as much as one order of magnitude can be achieved. This is the case for the sample deposited at 400 °C and −70 V (solid downward triangles). The conductivity values decrease again for samples deposited at −100 (open upward triangles) and −200 V (stars), where the values for the latter are of the same magnitude as in samples deposited at floating potential.

It is not surprising that the in-plane ionic conductivities should be the same in samples deposited at floating potential at 200 and 400 °C, respectively, considering that the substrate temperature did not influence the grain size and microstrain in the films. Additionally, no voids were observed in either film. Least squares fitting yielded slopes from which activation energies for oxygen ion migration in the range of 1.14–1.30 eV were obtained [Eq. (1)]. These values are somewhat higher than the activation energy for bulk migration in single crystal YSZ (~1.1 eV) with the same composition but within the error bars.[30]

We suggest that the ionic species ($O^{2-}$) migrate through grain boundaries in addition to bulk migration mediated by vacancies in the grain interior. This could explain why the in-plane ionic conductivity increases one order of magnitude for the film deposited at 400 °C and −70 V. It was observed that the grain size decreased in samples deposited at high bias voltages (cf. Fig. 3), which would mean that the grain-boundary density increased. As a result, the oxide ion transport along grain boundaries is accelerated and hence the ionic conductivity is significantly enhanced.[31] However, due to additional incorporation of Ar in samples deposited at even higher bias voltages (cf. Fig. 4), the Ar atoms may have segregated to the grain boundaries (cf. Fig. 5), thereby blocking the pathways for $O^{2-}$ ions. This explains why the in-plane ionic conductivities for samples deposited at 400 °C at −100 and −200 V, respectively, are lower than for the sample deposited at 400 °C and −70 V since the latter did not contain any Ar, as evidenced by RBS. From Fig. 3 it is not evident that the grain size (calculated from GIXRD) is smaller in the sample deposited at −70 V compared to the sample deposited at floating potential. However, the grain sizes determined from x-ray data in the $\theta$-$2\theta$ geometry showed that the grain sizes obtained for the 111 diffraction peak were ~18 and ~15 nm for samples deposited at 400 °C and floating potential and −70 V, respectively. This discrepancy is due to the different scattering geometries.

Our results show that in addition to bulk migration, oxygen ion migration along grain boundaries is also a likely mechanism for ionic conduction in magnetron-sputtered nanocrystalline YSZ films. Furthermore, the in-plane ionic conductivities seem to correlate to the volume fraction of grain boundaries in the films. We did not observe any systematic decrease in activation energy for oxygen ion migration as a function of decreasing grain size. In fact we obtained activation energies higher than the activation energy for bulk migration in single crystal YSZ.

Kosacki *et al.*,[32] who studied yttria (16%)-stabilized zirconia thin films prepared by a polymer precursor process on alumina substrates, found that the nanocrystalline materials exhibited two orders of magnitude higher conductivities

compared to conventional polycrystalline and single crystalline materials associated with a reduction in the activation energy for oxygen ion migration from 1.15 to 0.93 eV. They attributed these results to the dilution of impurities at grain boundaries in nanocrystalline oxides. We have one sample deposited at 400 °C and −70 V which exhibits one order of magnitude higher conductivity compared to the sample deposited at 400 °C and floating potential corresponding to a smaller grain size. Aoki *et al.* observed a sharp drop in the specific grain boundary conductivity of CaO-stabilized zirconia with increasing grain size and correlated this to an increase in silicate impurity coverage of the grain boundaries.[33] We observe a similar effect presumably due to Ar impurities distributed mainly along the grain boundaries.

These results support our conclusion that ionic conduction in nanocrystalline YSZ thin films occurs through a combination of bulk and grain-boundary migration.

## IV. CONCLUSIONS

This work has shown that the thermal stability and in-plane ionic conductivity of magnetron-sputtered nanocrystalline YSZ films depend on the initial deposition temperature and substrate bias voltage, respectively. Annealing showed that negligible grain growth occurred below 800 °C for samples deposited at 400 °C, so grain growth did not affect the ionic conductivity measurements. Furthermore, depositions at elevated temperatures (i.e., 200 and 400 °C) resulted in denser films compared to room-temperature depositions. Films deposited at floating potential had a grain size of ~20 nm and a microstrain of ~2% regardless of deposition temperature. Films deposited at 400 °C and substrate bias voltages from −70 to −200 V showed a reduced grain size for higher bias voltages yielding a grain size of ~6 nm and a microstrain of ~2.5% at −175 and −200 V with additional incorporation of argon.

From impedance measurements activation energies for oxygen ion migration in the range of 1.14–1.30 eV were obtained. The in-plane ionic conductivity was highest in the film deposited at 400 °C and a substrate bias of −70 V but decreased for samples deposited at −100 and −200 V, respectively, likely due to the incorporation of Ar which may have segregated to the grain boundaries. These results suggest that ionic conduction in nanocrystalline YSZ thin films occurs through both bulk and grain-boundary migrations.

## ACKNOWLEDGMENTS

The authors would like to thank Jacques Chevallier for technical assistance, Folmer Lyckegaard and Pia Bomholt for the TEM sample preparation, and the Danish Ministry of Science for financial support. P.E. acknowledges funding from the Carlsberg Foundation.

[1] S. P. S. Badwal and K. Foger, Ceram. Int. **22**, 257 (1996).
[2] B. C. H. Steele and A. Heinzel, Nature (London) **414**, 345 (2001).
[3] S. A. Barnett, Energy **15**, 1 (1990).
[4] J. Maier, Solid State Ionics **131**, 13 (2000).
[5] M. G. Bellino, D. G. Lamas, and N. E. Walsöe de Reca, Adv. Funct. Mater. **16**, 107 (2006).
[6] J. Maier, J. Eur. Ceram. Soc. **24**, 1251 (2004).
[7] A. V. Chadwick, Phys. Status Solidi A **204**, 631 (2007).
[8] G. Knöner, K. Reimann, R. Röwer, U. Södervall, and H.-E. Schaefer, Proc. Natl. Acad. Sci. U.S.A. **100**, 3870 (2003).
[9] U. Brossman, G. Knöner, H.-E. Schaefer, and R. Würschum, Rev. Adv. Mater. Sci. **6**, 7 (2004).
[10] J. Maier, Nature Mater. **4**, 805 (2005).
[11] W. Jung, J. L. Hertz, and H. Tuller, Acta Mater. **57**, 1399 (2009).
[12] N. Nakagawa, H. Yoshioka, C. Kuroda, and M. Ishida, Solid State Ionics **35**, 249 (1989).
[13] J. G. Jones, A. A. Voevodin, and J. S. Zabinski, Surf. Coat. Technol. **146-147**, 258 (2001).
[14] I. Kosacki, C. M. Rouleau, P. F. Becher, J. Bentley, and D. H. Lowndes, Solid State Ionics **176**, 1319 (2005).
[15] B. Hobein, F. Tietz, D. Stöver, and E. W. Kreutz, J. Power Sources **105**, 239 (2002).
[16] E. S. Thiele, L. S. Wang, T. O. Mason, and S. A. Barnett, J. Vac. Sci. Technol. A **9**, 3054 (1991).
[17] A. F. Jankowski and J. P. Hayes, Surf. Coat. Technol. **76-77**, 126 (1995).
[18] L. R. Doolittle, Nucl. Instrum. Methods Phys. Res. B **9**, 344 (1985).
[19] Diffrac$^{plus}$ TOPAS P 2.1, Bruker AXS GmbH D-76187 Karlsruhe, Germany, 2003.
[20] Th. H. de Keijser, J. I. Langford, E. J. Mittemeijer, and A. B. P. Vogels, J. Appl. Crystallogr. **15**, 308 (1982).
[21] ZSIMPWIN 3.21, EChem Software, Bruno Deum, Ann Arbor, Michigan, USA, 1999.
[22] JCPDS Card No. 82-1246.
[23] B. Rauschenbach and J. W. Gerlach, Cryst. Res. Technol. **35**, 675 (2000).
[24] I. Petrov, P. B. Barna, L. Hultman, and J. E. Greene, J. Vac. Sci. Technol. A **21**, S117 (2003).
[25] P. Yashar, J. Rechner, M. S. Wong, W. D. Sproul, and S. A. Barnett, Surf. Coat. Technol. **94-95**, 333 (1997).
[26] D. Dobrev, Thin Solid Films **92**, 41 (1982).
[27] L. Dong and D. J. Srolovitz, Appl. Phys. Lett. **75**, 584 (1999).
[28] M. W. Finnis, A. T. Paxton, M. Methfessel, and M. van Schilfgaarde, Phys. Rev. Lett. **81**, 5149 (1998).
[29] B. A. Boukamp, Solid State Ionics **20**, 31 (1986).
[30] M. Filal, C. Petot, M. Mokchah, C. Chateau, and J. L. Carpentier, Solid State Ionics **80**, 27 (1995).
[31] H. L. Tuller, Solid State Ionics **131**, 143 (2000).
[32] I. Kosacki, B. Gorman, and H. U. Anderson, in *Ionic and Mixed Conductors*, edited by T. A. Ramanarayanan, W. L. Worrell, H. L. Tuller, A. C. Kandkar, M. Mogensen, and W. Gopel (Electrochemical Society, New York, 1998), Vol. 3, p. 631.
[33] M. Aoki, Y.-M. Chiang, I. Kosacki, J.-R. Lee, H. L. Tuller, and Y. J. Liu, J. Am. Ceram. Soc. **79**, 1169 (1996).